DEPENDENCE OF THE MICROSTRUCTURE AND ELECTRICAL PROPERTIES OF TUNGSTEN OXIDE CERAMICS ON SYNTHESIS CONDITIONS

V. S. Yavtushenko, A. Yu. Lyashkov*

Oles Honchar Dnipro National University, Dnipro, Ukraine
**e-mail: alexdnu@ukr.net*

The influence of synthesis conditions on the microstructure and electrical properties of tungsten oxide (WO_3) ceramics is investigated. It is established that pure tungsten oxide undergoes a solid-state sintering process, and the onset temperature of densification decreases significantly after mechanical milling of the powder. This effect is attributed to the increase in Gibbs surface energy with decreasing particle size, which thermodynamically promotes sintering at lower temperatures. The density of ceramics sintered at 1200 °C for 2 h is found to be approximately 5.8 g/cm³, corresponding to about 80 % of the theoretical density. Scanning electron microscopy reveals a homogeneous microstructure with an average grain size of about 10 μm and no detectable secondary phases. Differential thermal analysis shows a sequence of phase transitions ($\gamma \rightarrow \beta \rightarrow \delta \rightarrow \varepsilon \rightarrow WO_{3-x}$) associated with changes in defect structure and oxygen stoichiometry. Electrical measurements demonstrate nonlinear current–voltage characteristics similar to those of varistor materials, which are attributed to the formation of intergranular potential barriers. With increasing sintering temperature, the nonlinearity coefficient increases while the low-field conductivity decreases, indicating the strengthening of barrier effects at grain boundaries. The results confirm the potential of pure WO_3 ceramics as a base material for varistor and composite systems with nonlinear electrical behavior.

Keywords: tungsten oxide, WO_3, ceramics, sintering, microstructure, electrical properties, varistor.

Received 15.10.2025; Received in revised form 07.11.2025; Accepted 14.11.2025

1. Introduction

WO_3 is a typical transition metal oxide whose electronic properties are highly sensitive to the concentration of oxygen vacancies. Even minor changes in oxygen content result in significant variations in electrical conductivity and dielectric properties, making WO_3 extremely sensitive to synthesis and processing conditions [1]. For pressed, granulated WO_3 powder ceramics, typical sintering temperatures reported in the literature range from approximately 600 to 1100 °C, depending on sintering duration, initial green density, and atmosphere. At the lower end of this range, incomplete densification and high porosity are observed, while higher temperatures promote grain growth and may induce phase transformations [2].

The sintering atmosphere (air, oxygen, or reducing environment) critically affects the concentration of oxygen vacancies. An oxidative atmosphere decreases the number of vacancies and preserves insulating behavior, whereas a reducing atmosphere generates n-type conductivity via donor vacancies and increases electrical conductivity. It has been reported that reduction even at relatively low temperatures substantially enhances conductivity [2]. In pure WO_3, the electrical conductivity is typically n-type, arising from electrons released from oxygen vacancies. Each defect configuration associated with vacancies can contribute one or more electrons to the conduction band, depending on the specific crystal phase and local chemical environment [3].

To explain the conduction mechanisms of tungsten oxide over a wide temperature range, several processes are considered: small-polaron hopping at low temperatures, thermally activated conduction at intermediate and high temperatures, and donor-type conduction. The frequency- and temperature-dependent behavior of the complex dielectric permittivity often reflects signatures of polaron localization and grain-boundary relaxation [4].

Tungsten oxide is relatively difficult to fully densify without the addition of sintering aids or fluxes. The absence of liquid-phase processes at moderate temperatures hinders grain growth and limits densification at elevated temperatures. Thermodynamic stability and potential reduction to sub-oxides under reducing conditions are also critical considerations.

Consequently, additives are often employed in practice, but these approaches are not applicable for pure WO_3 materials [5].

WO_3 exhibits multiple crystalline modifications (monoclinic, triclinic, tetragonal, etc.), and the phase composition depends on temperature, grain size, and sintering conditions. Mixed-phase compositions are commonly observed in ceramics sintered between 600 and 1000 °C. Changes in microstructure can be accompanied by phase transitions [6]. Phase transformations during heating, cooling, or grain growth are associated with modifications of the electronic structure and electrical properties [7].

For nanostructures obtained by various methods, reported particle sizes range from tens of nanometers to several hundred nanometers, extending to > 1 μm for high-temperature sintering. Increasing the sintering temperature leads to pronounced grain growth and a reduction in porosity [8]. Grain boundaries and pores act as local charge and vacancy traps; the distribution of vacancies across the bulk and surface is a primary source of local variability in electrical properties [2].

Several studies [9-10] have proposed using a polymeric positive temperature coefficient (PPTC) device in thermal contact with a varistor to protect solar cells from "hot spots." Such localized overheating occurs when individual photovoltaic cells overheat and act as loads, drawing energy from illuminated cells, which may result in physical damage or even fire [11]. The typical output voltage of solar modules (usually 18–36 V) necessitates the use of varistors with low rated voltages. Consequently, WO_3-based varistors are considered promising components for such applications. Reference [12] investigated the possibility of combining PPTC and varistor functionalities in a single component by creating polyethylene-WO_3 ceramic composites. These materials exhibited both a positive temperature coefficient of resistance and nonlinear current-voltage characteristics. Optimizing the performance and stability of such composites requires the development of WO_3 ceramic processing technology as a foundational material for these applications.

The aim of the present study was to investigate the sintering behavior of tungsten oxide, its microstructure, and electrical properties under different synthesis conditions.

2. Experimental methodology, results and discussion

High-purity WO_3 powder was pressed into disk-shaped pellets under a pressure of 200 MPa. The samples were subsequently sintered in air while monitoring their relative linear shrinkage ($\Delta l/l_0$) during heating, where l_0 is the initial sample thickness, l is the final thickness, and $\Delta l = l - l_0$. Thickness measurements were performed photometrically without interrupting the sintering process. As shown in Fig. 1 (curve 1), the as-received powder exhibited negligible shrinkage up to 1300 °C, indicating practically no densification. The slight increase in sample thickness during heating is attributed to thermal expansion.

To enhance sintering behavior, the WO_3 powder was subjected to the same processing as used in varistor ceramic fabrication, namely ball milling in ethanol (C_2H_5OH). The corresponding shrinkage of milled samples is shown in Fig. 1 (curve 2). Shrinkage began at temperatures above 1000 °C; however, the resulting ceramics still exhibited relatively low mechanical strength. The density of ceramics sintered at 1200 °C for 2 h, calculated from geometric dimensions and mass, was 5.8 g/cm³, corresponding to approximately 80 % of the theoretical WO_3 density. The final relative shrinkage $\Delta l/l_0$ reached 10.8 %.

Scanning electron microscopy revealed that the as-received powder consisted of relatively coarse particles ranging from 10 to 100 μm (Fig. 2a). After milling, a large fraction of fine particles (< 1 μm) appeared, although some coarser particles remained (Fig. 2b). Sintering at 1200 °C for 2 h resulted in a fairly homogeneous microstructure typical of

ceramic materials [13], with an average grain size of approximately 10 μm (Fig. 2c). Microstructural analysis of polished cross-sections further confirmed the ceramic nature of the material (Fig. 3). No secondary phases were detected between grains by energy-dispersive X-ray spectroscopy (EDX), indicating that the sintering mechanism was solid-state.

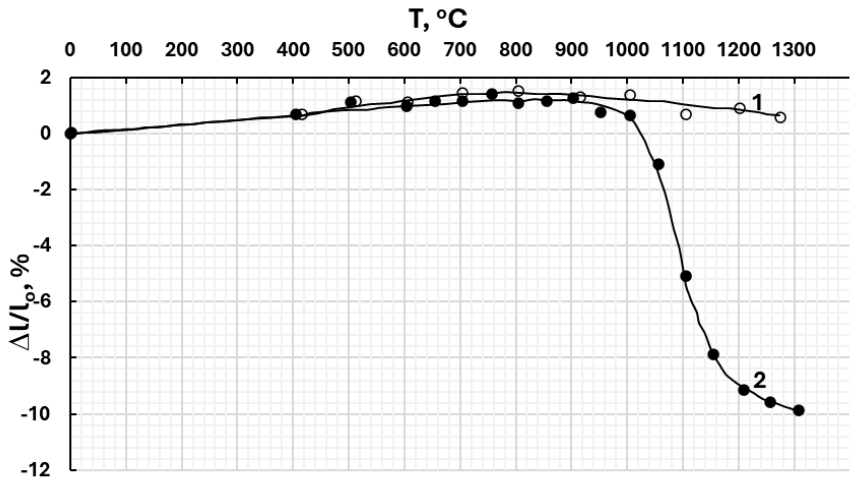

Fig. 1. Relative change in the geometric dimensions of pressed WO_3 samples during sintering (heating rate 10 °C/min).
1 – as-received WO_3; 2 – milled WO_3

The reduction in sintering temperature for milled powders is explained by the increased Gibbs surface energy of finer grains. Thermodynamically, the system tends to minimize surface energy, which promotes densification at lower temperatures for fine-grained materials [14-15].

A question arises regarding the absence of coarse grains in the sintered ceramics, despite their presence in the starting powder. This can be explained by the polymorphic phase transition of WO_3 at 740 °C, which involves a sudden change in lattice parameters and leads to cracking of large particles during heating.

Differential thermal analysis (DTA) of WO_3 revealed a series of characteristic thermal effects corresponding to sequential structural and stoichiometric transformations of the material (Fig. 4). An exothermic peak at approximately 450 °C is associated with the crystallization of amorphous or poorly ordered oxide and the formation of the monoclinic γ-WO_3 phase; this process is accompanied by the release of heat due to structural ordering. Around 580 °C, a broad endothermic effect corresponds to the polymorphic transition γ-WO_3 → β-WO_3 (monoclinic → orthorhombic modification) and partial disordering of the oxygen sublattice. In the 580-1000 °C range, a broad combined exothermic maximum with a peak near 820 °C is observed, reflecting overlapping processes of recrystallization, β→δ→ε transitions, and the formation of defective WO_{3-x} regions with localized structural relaxation. Narrow endothermic peaks at 800 °C and 950 °C correspond to high-temperature structural transitions and partial oxygen loss from the lattice, leading to defect-rich phases with reduced oxygen content. Together, these processes produce a complex thermal profile for WO_3, where temperature extrema result from both phase transitions between crystalline modifications and defect–reduction phenomena during heating [7, 16-17].

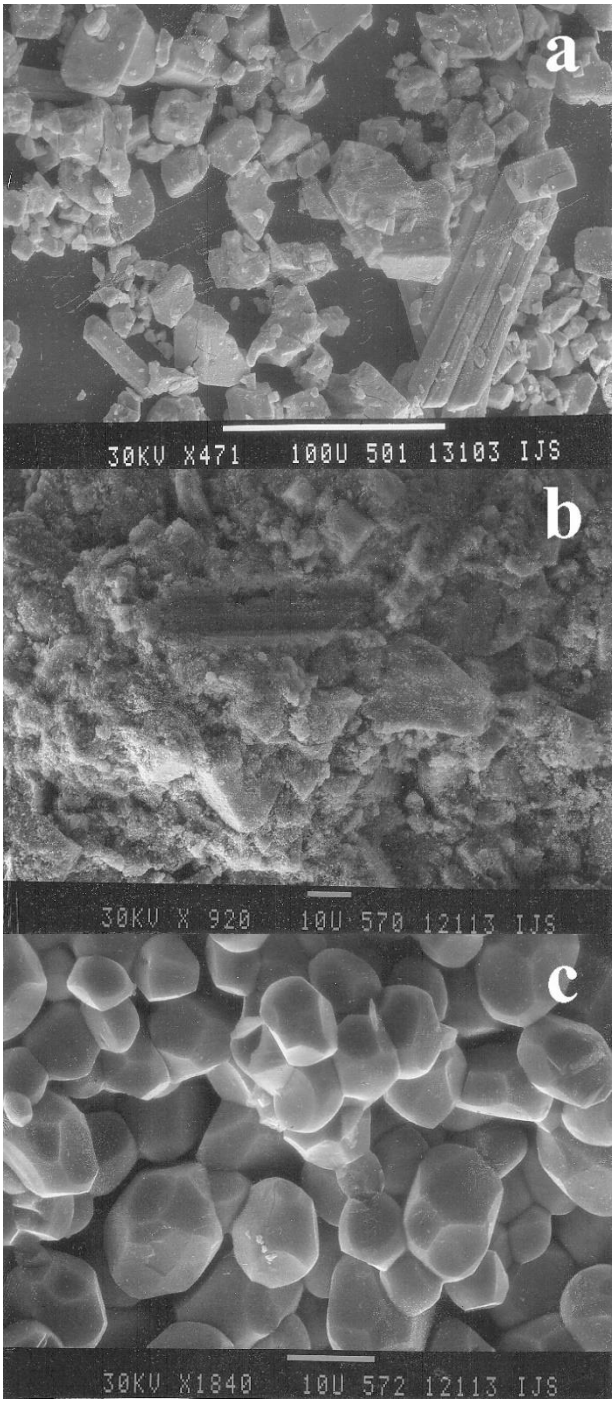

Fig. 2. SEM micrographs of (a) as-received WO_3 powder, (b) milled WO_3 powder, and (c) WO_3 ceramic sintered at 1200 °C for 2 h (fracture surface).

The current-voltage characteristics (I–V characteristics) of sintered WO_3 were found to be nonlinear (Fig. 5). Samples sintered at 1250 °C exhibited lower electrical conductivity than those sintered at 1200 °C. The activation energy of conduction in ceramic WO_3 over the

– 70-30 °C range was 0.27 eV during heating and 0.29 eV during cooling. A conductivity hysteresis of approximately 0.6 orders of magnitude between heating and cooling is attributed to water desorption from grain surfaces.

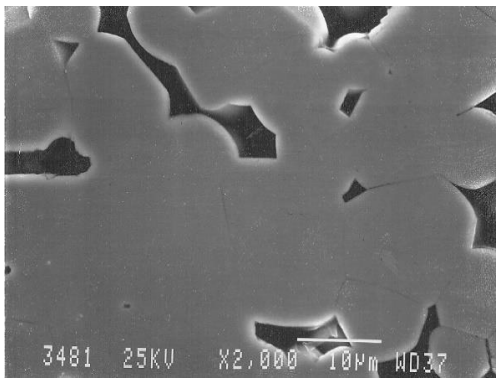

Fig. 3. SEM micrographs of WO_3 ceramic sintered at 1200 °C for 2 h (polished cross-section).

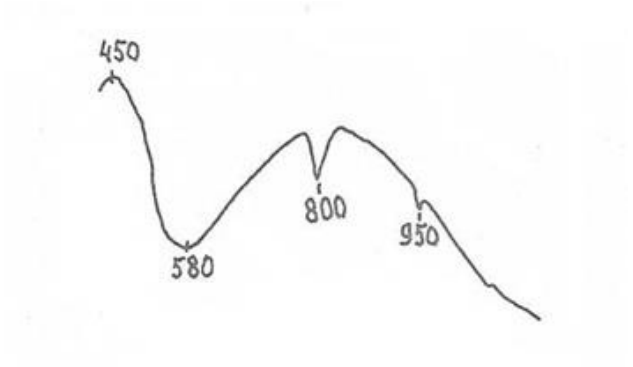

Fig. 4. Differential thermal analysis (DTA) of WO_3 (temperatures in °C).

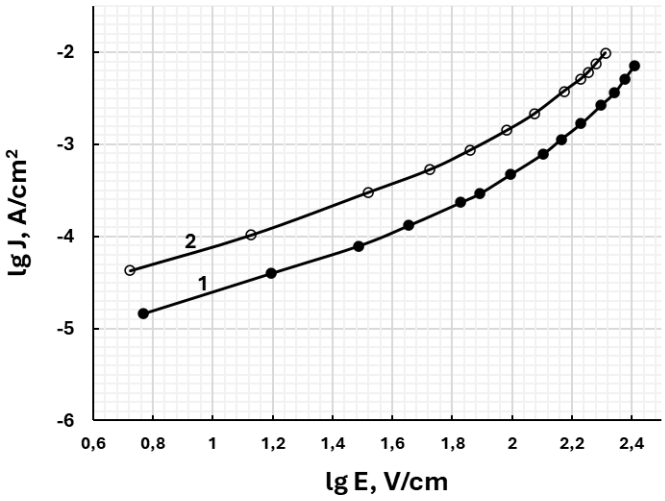

1 – 1250 °C; 2 – 1200 °C

Fig. 5. Current-voltage characteristics (CVCs) of WO_3 sintered at different temperatures for 2 h.

The nonlinearity coefficient (α) of the current–voltage characteristics (I–V characteristics) was calculated according to the expression

$$\alpha = \frac{\lg(J_2/J_1)}{\lg(U_2/U_1)},$$

where $J_1 = 0.1\,\text{mA/cm}^2$, $J_2 = 1\,\text{mA/cm}^2$, and U_1, U_2 are the corresponding voltages [18-19]. The coefficient α gradually increases from values close to 1 for samples sintered at 1100 °C to about 2 at 1250 °C (Fig. 6, curve 1).

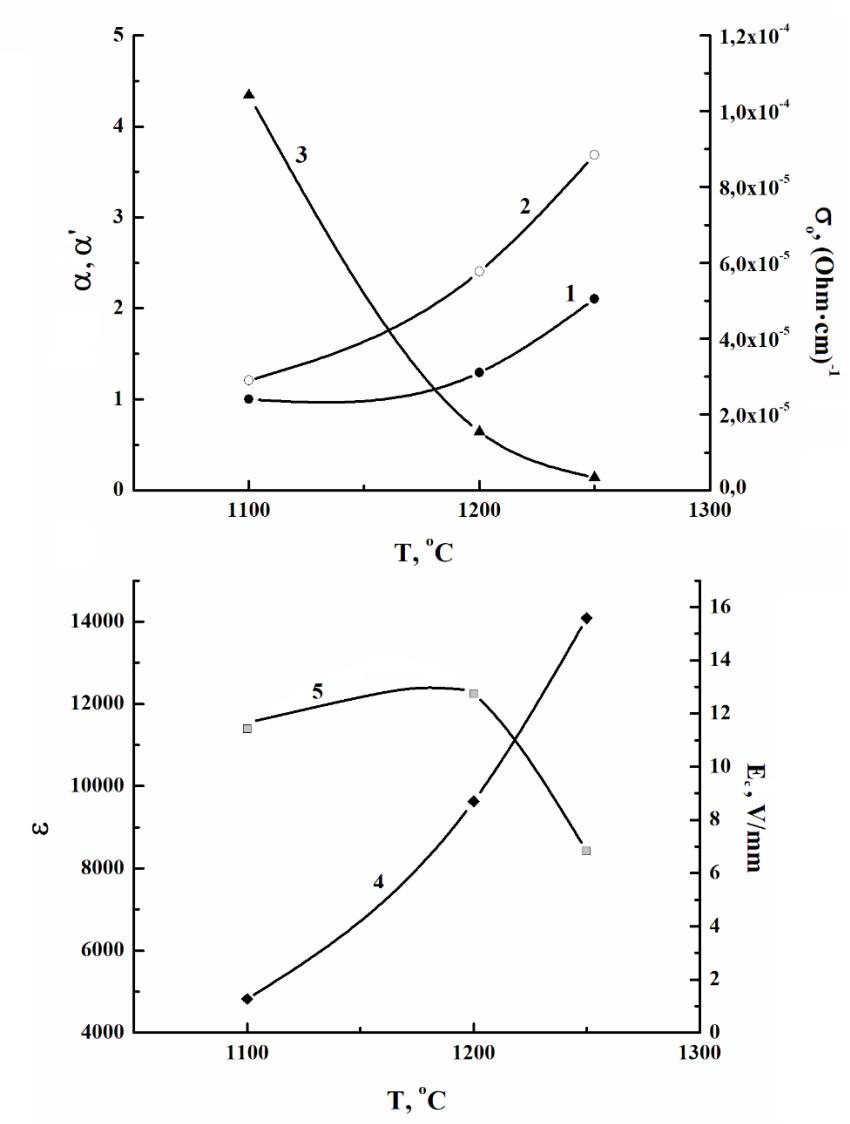

Fig. 6. Dependence of electrical parameters of WO_3 on sintering temperature (2 h).
1 – nonlinearity coefficient α in the current density range 0.1-1 mA/cm²; 2 – nonlinearity coefficient α′ in the current density range 1-10 mA/cm²; 3 – low-field electrical conductivity σ_o; 4 – electric field E at 1 mA/cm²; 5 – dielectric permittivity ε at 1 kHz.

The nonlinearity coefficient determined in the current density range of 1–10 mA/cm^2 (denoted as α') varies from 1.2 to 3.7 and also increases with sintering temperature. Throughout the investigated range, $\alpha' > \alpha$ (Fig. 6, curve 1), which reflects an enhancement in the steepness of the I–V characteristics with increasing electric field strength.

The specific electrical conductivity in a weak electric field (σ_0) decreases with increasing sintering temperature from 10^{-4} (Ohm · cm)$^{-1}$ at 1100 °C to 3.4×10^{-6} (Ohm · cm)$^{-1}$ at 1250 °C (Fig. 6, curve 3). The electric field strength at a current density of 1 mA/cm^2 (E_c) rises from 1.3 V/mm to 3.7 V/mm with increasing sintering temperature (Fig. 6, curve 4).

These results indicate the formation of intergranular potential barriers (IPBs) at the grain boundaries of WO_3, analogous to those observed in ZnO-based varistor ceramics [20]. Such barriers arise due to chemisorption of oxygen in charged forms on the grain surface, leading to local depletion of charge carriers, while the grain core remains relatively conductive. Based on the obtained data, it can be inferred that the barrier height increases with sintering temperature, which correlates well with the trends in α, α', σ_0, and E_c.

The microstructure of the WO_3 ceramics also supports the existence of IPBs – the grains are well-defined, and no "bridge-like" necks are observed between them that could allow current to bypass the depleted boundary regions. The high dielectric permittivity values (Fig. 6, curve 5) ($\varepsilon \approx 1200$-8000) are consistent with a space-charge polarization mechanism typical of varistor-type materials with charge-depleted grain surfaces [21]. The relative decrease in ε for ceramics sintered at 1250 °C can be attributed to grain coarsening, which reduces the number of parallel "capacitors" formed by the conductive grain–IPB–conductive grain structure. Another possible explanation is the thickening of the depletion region due to an increase in the IPB height.

Conclusions

It was established that the sintering of pure WO_3 proceeds via a solid-state mechanism without the formation of a liquid phase; densification begins at temperatures above 1000 °C.

Preliminary milling of the powder reduces the sintering temperature due to the increase in Gibbs surface energy of fine particles, which enhances diffusion processes and promotes densification.

WO_3 ceramics sintered at 1200 °C exhibit a density of approximately 5.8 g/cm³ (≈ 80 % of the theoretical value) and possess a uniform microstructure with an average grain size of about 10 μm and no secondary phases.

Thermal analysis revealed a series of phase transitions and defect–reduction processes accompanied by changes in oxygen stoichiometry and crystal structure.

Electrical characterization showed nonlinear current-voltage behavior, indicating the formation of intergranular potential barriers similar to those in ZnO-based varistor ceramics.

Increasing the sintering temperature leads to a higher nonlinearity coefficient (α) and lower electrical conductivity, which corresponds to higher potential barrier heights at grain boundaries.

The observed dependence of electrical properties on microstructure confirms the applicability of WO_3 ceramics as a base material for varistors and composite systems with a positive temperature coefficient of resistance (PPTC).

References

1. **Yao, Y.** A review on the properties and applications of WO_3 nanostructure-based optical and electronic devices / Y. Yao, D. Sang, L. Zou, Q. Wang, C. Liu // Nanomaterials. – 2021. – Vol. 11(8). – P. 2136. DOI: 10.3390/nano11082136

2. **Souza Filho, A. G.** Microstructural and electrical properties of sintered tungsten trioxide / A. G. Souza Filho, J. G. N. Matias, N. L. Dias, V. N. Freire, J. F. Julião, U. U. Gomes // Journal of Materials Science. – 1999. – Vol. 34(5). – P. 1031 – 1035. DOI: 10.1023/A:1004544011638

3. **Chatten, R.** The oxygen vacancy in crystal phases of WO_3 / R. Chatten, A. V. Chadwick, A. Rougier, P. J. Lindan // J. Phys. Chem. B. – 2005. – Vol. 109(8). – P. 3146 – 3156.
DOI: 10.1021/jp045655r

4. **Nehra, P.** Electrical conduction mechanisms in Gd-substituted WO_3 ceramics: experimental and theoretical approaches / P. Nehra, P. S. Rana, S. Singh // J. Phys. Chem. C. – 2024. – Vol. 128(19). – P. 8085 – 8094. DOI: 10.1021/acs.jpcc.4c01280

5. **Miyazaki, H.** Effects of a B_2O_3 additive on the sintering properties of WO_3 ceramics. / Miyazaki, H., Ando, J., Nose, A., Suzuki, H., Ota, T. // Materials research bulletin. – 2015. – Vol. 64. – P. 233 –235. DOI: 10.1016/j.materresbull.2014.12.076

6. **Souza-Filho, A. G.** Coexistence of triclinic and monoclinic phases in WO_3 ceramics / A. G. Souza-Filho, V. N. Freire, J. M. Sasaki, J. Mendes Filho, J. F. Julião, U. U. Gomes // J. Raman Spectrosc. – 2000. – Vol. 31(6). – P. 451 – 454.
DOI: 10.1002/1097-4555(200006)31:6<451::AID-JRS528>3.0.CO;2-K

7. **Ramana, C. V.** Structural stability and phase transitions in WO_3 thin films / C. V. Ramana, S. Utsunomiya, R. C. Ewing, C. M. Julien, U. Becker // J. Phys. Chem. B. – 2006. – Vol. 110(21). – P. 10430–10435. DOI: 10.1021/jp056664i

8. **Pandey, N. K.** Synthesis and characterization of WO_3 nanomaterials / N. K. Pandey, K. Tiwari, A. Roy // J. Biomed. Nanotechnol. – 2011. – Vol. 7(1). – P. 156 – 157. DOI: 10.1166/jbn.2011.1247

9. **Tonkoshkur, A.** Algorithm for software implementation of designing overvoltage protection in photovoltaic modules of solar arrays using a varistor-posistor structure / A. Tonkoshkur, A. Ivanchenko // System Technologies. – 2020. – Vol. 1(126). – P. 124 – 143. DOI: 10.34185/1562-9945-1-126-2020-14

10. **Tonkoshkur, A. S.** Modeling of voltage-limiting kinetics in two-layer varistor–posistor structures / A. S. Tonkoshkur, A. V. Ivanchenko // Multidiscipline Modeling in Materials and Structures. – 2023. – Vol. 19(6). – P. 1249 – 1261. DOI: 10.1108/MMMS-11-2022-0249

11. **Dhimish, M.** Photovoltaic hotspots: a mitigation technique and its thermal cycle / M. Dhimish, M. Theristis, V. d'Alessandro // Optik. – 2024. – Vol. 300. – P. 171627.
DOI: 10.1016/j.ijleo.2024.171627

12. **Lyashkov, A. Y.** Structure and electrical properties of polymer composites based on tungsten oxide varistor ceramics / A. Y. Lyashkov, V. O. Makarov, Y. G. Plakhtii // Ceramics International. – 2022. – Vol. 48(6). – P. 8306 – 8313. DOI: 10.1016/j.ceramint.2021.12.035

13. **Hongwang, Z.** Origin of varistor properties of tungsten trioxide (WO_3) ceramics / Z. Hongwang, H. Zhongqiu, L. Tongye, W. Yu, Z. Yong // J. Semiconductors. – 2010. – Vol. 31(2). – P. 023001. DOI: 10.1088/1674-4926/31/2/023001

14. **Parker, S. C.** Kinetic model for sintering of supported metal particles with improved size-dependent energetics and applications to Au on TiO_2(110) / S. C. Parker, C. T.

Campbell // Phys. Rev. B. – 2007. – Vol. 75. – P. 035430. DOI: 10.1103/PhysRevB.75.035430

15. **Jiang, J.** The effect of heating rate on the sintering of aluminum nanospheres / J. Jiang, Y. Chen, T. Zhang, X. Li // Phys. Chem. Chem. Phys. – 2021. – Vol. 23(5). – P. 2921 – 2928.
DOI: 10.1039/D0CP06669A

16. **Han, B.-Y.** WO_3 thermodynamic properties at 80–1256 K revisited / B.-Y. Han, H.-L. Sun, Y. Zhou, Q.-G. Zhu // J. Therm. Anal. Calorim. – 2020. – Vol. 142. – P. 2057 – 2065. DOI: 10.1007/s10973-020-09345-z

17. **Guo, W.** A Bulk Oxygen Vacancy Dominating WO_{3-x} Photocatalyst for Carbamazepine Degradation / W. Guo, Q. Wei, G. Li, F. Wei, Z. Hu // Nanomaterials. – 2024. – Vol. 14(11). – P. 923. DOI: 10.3390/nano14110923

18. **Makarov, V. O.** Sintering and electrical conductivity of doped WO_3 / V. O. Makarov, M. Trontelj // Journal of the European Ceramic Society. – 1996. – Vol. 16(7). – P. 791 – 794.
DOI: 10.1016/0955-2219(95)00204-9

19. **Canessa, E.** Non-linear I–V characteristics of double Schottky barriers and polycrystalline semiconductors / E. Canessa, V. L. Nguyen // Physica B: Condensed Matter. – 1992. – Vol. 179(4). – P. 335-341. DOI: 10.1016/0921-4526(92)90634-5

20. **Oliveira, M. M.** WO_3-based varistors – a review / M. M. Oliveira, P. A. P. Pessoa, R. L. Brito, J. H. G. Rangel, J. S. Vasconcelos, E. Longo // Matéria (Rio de Janeiro). – 2016. – Vol. 21. – P. 105 –114. DOI: 10.1590/S1517-707620160001.0010

21. **Tonkoshkur, A. S.** Basic models in dielectric spectroscopy of heterogeneous materials with semiconductor inclusions / A. S. Tonkoshkur, A. B. Glot, A. V. Ivanchenko // Multidiscipline Modeling in Materials and Structures. – 2017. – Vol. 13(1). – P. 36 – 57. DOI: 10.1108/MMMS-08-2016-0037